Research Article | Vol. 27, No. 18 | 2 Sep 2019 | OPTICS EXPRESS 25912
Optics EXPRESS

3D nanoporous antennas as a platform for high sensitivity IR plasmonic sensing

EUGENIO CALANDRINI, GIORGIA GIOVANNINI, AND DENIS GAROLI*

Istituto Italiano di Tecnologia, Via Morego 30, 16136 Genova, Italy
**denis.garoli@iit.it*

Abstract: Nanoporous gold can be exploited as plasmonic material for enhanced spectroscopy both in the visible and in the near-infrared spectral regions. In particular, the peculiar morphology of such a substrate leads to a higher field confinement with respect to conventional plasmonic materials. This property can be exploited to achieve extremely high sensitivity to the changes in environmental conditions, making it an interesting tool for the development of sensors and biosensors. Here, we compared the sensitivity of a plasmonic resonator made of nanoporous gold with a similar structure made of homogeneous gold. To assess the enhanced sensitivity the same stoichiometric quantity of dielectric material was deposited via Atomic Layer Deposition onto the two considered structures. Experimental results proved the higher sensitivity was achievable using nanoporous gold. In particular, such 3D nanoporous structures can be proposed as a promising sensing platform in the near-infrared with a sensitivity over 4.000 nm/RIU.

1. Introduction

One of the most striking achievements pursued by plasmonics in optics is the enhancement of sensors sensitivity to detect molecular binding events and changes in molecular conformation [1–7]. The sensitivity of these sensors is given by the ratio between the spectral shift of the plasmon resonance ($\Delta\lambda$) and the refractive index (Δn). This values can vary in presence of the analyte due to the changes in the environmental conditions surrounding the plasmonic sensor. A key parameter used to characterize the SPR sensor performances is the detection limit, defined as the minimum amount of analyte detectable by the sensor, which is expressed in Refractive Index Units (RIU). Several schemes have been successfully proposed, exploiting both the Surface Plasmon Polariton (SPP) and the Localized Surface Plasmon Resonance (LSPR) [8]. In the first case, propagating plasmons are launched on metal surfaces through the coupling with a prism [9]. The replacement of the bulky prism-coupling mechanism with ordered nanostructures like grooves or slits prepared on the metal surface provide the effective excitation of (SPP) at (near) normal incidence. This allows the implementation of a microarray format for multiplexed and high-throughput biosensing platform [10]. Furthermore, their operation in transmission/reflectance configurations makes them eligible for the integration in imaging-based devices [11]. On the other hand, nanoparticles with different sizes and shapes, either dispersed in colloidal solution [12] or fabricated on substrates by lithography [13,14], support localized plasmons. Plasmonic nanoparticles supporting LSPR displays greater spatial resolution, both lateral and normal, when compared with SPP and a scattering cross-section remarkably greater than the fluorescence cross-section of fluorophores. Moreover, they do not blink or bleach, providing a virtually unlimited photon resource for observing molecular binding over arbitrarily long time intervals. A complete review of LSPR-based sensors can be found in [15]. In both configurations, LSPR or SPP, plasmonic architectures allow the subwavelength light confinement and enhancement near the metallic surface as a result of electromagnetic waves coupling to electrons. Since the resonance (and existence) conditions for these structures depend on the dielectric permittivity of the environment in contact to the surface of the metal, it turns out that plasmonics based detection is a refractometric

#368569 https://doi.org/10.1364/OE.27.025912
Journal © 2019 Received 27 May 2019; revised 20 Jul 2019; accepted 20 Jul 2019; published 28 Aug 2019

Optics EXPRESS

measurement that responds to changes in the effective refractive index within the surface plasmon decay length. This latter dimension can span between few to tens of nanometers depending on the working wavelength and on the structure design. Sensitivity of state-of-the-art plasmonic sensor typically peaks at 1000 nm/RIU [16–18], and can even increases up to 30.000 nm/RIU when plasmonic metamaterials are employed [19,20]. Unfortunately, this result was recorded exploiting a sensing mechanism based on the bulk Kretschmann configuration that is hardly miniaturized for commercial biosensors [21]. Recently we have shown that Nanoporous Gold (NPG) enables higher field confinement with respect to conventional homogeneous materials like gold and silver [22,23], especially in the near-infrared (NIR) spectral region. Moreover, considering the higher surface/volume ration and therefore the large area available for the analyte-sensor interaction, these porous material become extremely interesting for high-sensitivity sensing. In particular we have recently demonstrated that the optical/plasmonic properties of NPG in the NIR can be exploited as a high performance sensing platform with sensitivity close to 15.000 nm/RIU [24]. Even though state-of-the-art platforms showed even higher sensitivity [19,20], this latter has been demonstrated in a very simple configuration where the spectral shifts of the NPG plasma edge were monitored during successive functionalization steps with organic or dielectric molecules.

Here we want to explore the NPG's sensing capability in the case of plasmonic resonators. In particular, considering our previous investigation on NPG 3D antennas [23], we build an SPR platform based on these structure for sensing in the NIR, and we compare its performance with the one obtained with a similar structure prepared in homogeneous gold. We achieved a sensitivity over $4x10^3$ nm/RIU by depositing conformal layer of SiO_2 on the NPG antennas. Moreover, we confirmed the good performance of the platform by detecting a small peptide (7-hystidine) at concentrations comparable to the one used in our previous work [24]..

2. Materials and methods

2.1 Optical spectroscopy

The optical response in the IR range was investigated by means of Fourier Transform Infrared (FT-IR) reflectance microscopy [25] measurements by using a Nicolet iS 50 FT-IR Spectrometer coupled to the Nicolet Continuμm Infrared Microscope by Thermo Scientific. A gold mirror was used as reference. The dielectric permittivity (ε) of this effective porous conductor was extracted through a fit of the measured reflectivity spectra within the Drude-Lorentz model. The optical response was characterized by a reduction of the absolute values of ε with respect to the homogeneous counterpart, mitigating the optical losses and increasing the skin depth, thus enabling the penetration of the electromagnetic field deeply into the porous matrix loaded with the analyte to be detected. FTIR microspectroscopy with a 30° incidence Cassegrain objective in the reflection mode was employed to compare the far field optical response of two different chip of 3D vertical antennas made by nanoporous gold and homogenous gold in a SPR configuration

2.2 Refractive index calculation

In the case of SiO_2 deposition, the refractive index variation Δn was empirically calculated under the following assumption: the film covered by the SiO_2 can be thought of as Insulator-Metal multilayered metamaterial, which overall effective dielectric function was dominated by the component longitudinal to the film plane. This can be easily calculated by applying the interface conditions for the electric field vector. The dielectric functions used for these estimations are found in literature for gold and silicon dioxide, while for NPG the previously calculated [24] dielectric function was used. The treatment of the optical response of the NPG film was carried out in the framework of the effective medium approximation. Within this context NPG is considered as a continuous layer with an effective dielectric function determined by the Drude-Lorentz model. The SiO_2 layer is treated as a continuous layer

Optics EXPRESS

covering the NPG effective metal. A multilayer model gives a fair estimation of the refractive index change, described by the following relation (The complete analysis is reported in [24]):

$$\Delta n = \sqrt{\varepsilon_{NPG}} - \sqrt{\varepsilon^{//}_{avg}} = \sqrt{\varepsilon_{NPG}} - \sqrt{\frac{\varepsilon_{NPG} t_{NPG} + \varepsilon_{SiO2} t_{SiO2}}{t_{NPG} + t_{SiO2}}} \quad (1)$$

Where ε_{NPG}, ε_{avg}, ε_{SiO2}, are the dielectric constants of NPG, the SiO_2/NPG by-layer, and SiO_2, respectively. Finally, t_{NPG} and t_{SiO2} are the thickness of the layers.

2.3 Surface functionalization protocol for dry sensing experiments

The NPG surface was firstly covered by depositing a monolayer of (3-Aminopropyl)triethoxysilane (APTES) by Atomic Layer Deposition (ALD; model FlexAl from Oxford Instruments) self-limited deposition of single layer. The APTES (Sigma-Aldrich bubbler PubChem Substance ID 24867571) was heated at 60°C and the precursor vapor was delivered into the chamber using 100 sccm of Argon. Precursor delivering lines were heated at 110°C, the chamber was at 120°C and substrate temperature was at 110°C. Chamber pressure during the process was maintained at 200 torr with 100 sccm of Argon. The process consisted of 40 cycles of 30" precursor exposure step followed by 30" of purging step using Argon as purging gas. The surface was then incubated for two hours at 40°C with 5mM (5mL) solution of succinic anhydride (>99%, Sigma Aldrich) in water. The surface was washed with water (5mL) to remove the unreacted anhydride, and the carboxyl groups thus exposed at the surface were activated with 5mM EDC (>99%, Sigma Aldrich) 5mM NHS (>98%, Sigma Aldrich) solution for 30 minutes at room temperature (R.T.). The coupling reagents were removed by flushing the surface with water. The surface was then treated with 10, 1, 0.1 and 0.01 nM solution of ployhistidine h at R.T. After 2 hours, the surface was washed once and analysed in dry condition.

3. Results and discussion

High aspect ratio plasmonic nanostructures have been extensively investigated for sensing [23,26,27]. Here, we report on 3D antennas described in details in Ref [23]. Two samples of vertical antennas protruding from a silicon nitride membranes made of optical resist hardened by means Focused Ion Beam (FIB) lithography are coated by 80 nm thick NPG layer and 25 nm thick gold layer, respectively. NPG porous density was tuned through a chemical etching reaction of an AuAg alloy rich in Ag in order to display a plasma frequency in the near infrared region of the electromagnetic spectrum. This has been done with a 1.5 hours dealloying process in HNO_3 [23] (To note that different porosity can be prepared with a longer dealloying time. Unfortunately this has been observed to be critical due to poor adhesion of porous metal on the antenna's scaffold) SEM micrographs of the prepared samples are reported in Fig. 1 in comparison with the same structure prepared with homogeneous gold (in the inset). This type of structures can sustain SPR resonance when illuminated by an electromagnetic wave with a non-vanishing component polarized along the antenna axis (p-polarization). The resonance wavelength is mainly set by the length and the pitch of the antennas in the array [28–31]. In our experiments we prepared vertical antennas with a height of 500 nm, a pitch of 1.25 μm and a diameter of 280 nm and 180 nm for NPG and homogeneous gold, respectively. This gives a plasmonic resonance at around 2300 nm. It is worth noting, in order to prepare a porous antennas with good morphology, a minimum thickness of 80 nm is required for NPG. This limits the aspect ratio that can be achieved with this structure which affects the quality factor of the resonance.

Optics EXPRESS

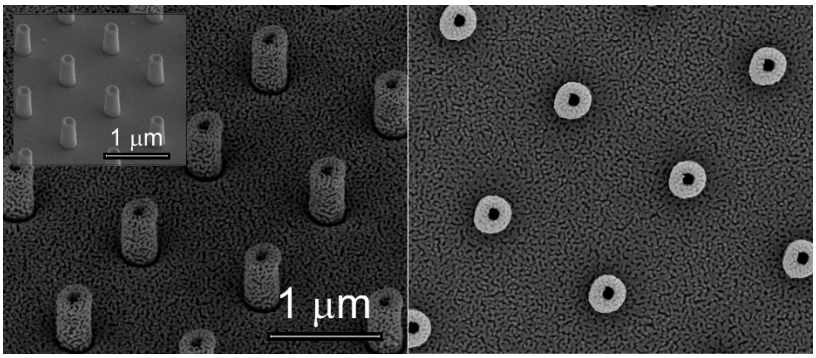

Fig. 1. SEM micrographs of NPG vertical antennas (top and tilted views). Inset: tilted view of the same structure prepared in homogeneous gold.

The bare structures have been characterized by means of FTIR and successively additional layers of SiO_2 have been deposited via ALD with steps of 1.4 nm putting the two samples (NPG and homogeneous gold) in the deposition chamber at the same time. As already mentioned, the intrinsic properties of ALD ensure stoichiometric depositions of the same amount of molecules onto the two substrates [32,33], hence allowing a direct comparison of the sensing performance without considering the higher surface/volume of NPG. The result of the measurement is illustrated in Fig. 2(a) for both the NPG and the homogeneous gold, used here as a reference. The two antenna arrays were optimized to resonate at the same wavelength, within the fabrication accuracy. In this condition, the wavelength dependency of the refractive indexes of the employed materials - Au, NPG, SiO_2 -can be disregarded. The antenna resonances display a quality factor of 12.7 and 7.4 for homogeneous gold and NPG, respectively. In this case, the antenna diameter through the aspect ratio can play a major role on the resonance quality factor. Following the minimum of the resonance dip as a function of the thickness of the SiO_2 layer, the spectral shift was calculated and plotted in Fig. 2(b) for the two arrays. The overall spectral shift for the NPG array is more than two-fold with respect the Au array and it is significant even for thicknesses around 1 nm. This highlights that the possibility of tuning the dielectric function of the plasmonic material allows to remarkably increase the sensitivity of plasmonic-based sensing devices.

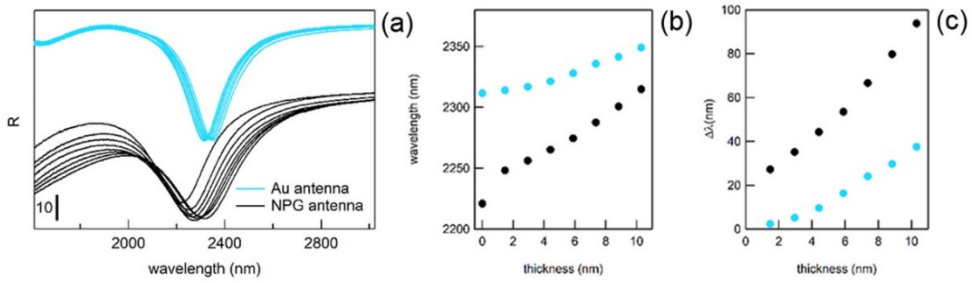

Fig. 2. (a)Reflectance curves of 3D antenna arrays for NPG and homogeneous gold. (b) Resonance wavelength and (c) spectral shift as a function of the thickness of the SiO_2 layer.

In order to evaluate the sensing performance of this system, the refractive index sensitivity S and the figure of merit (FoM) are introduced [34,35]. The first is defined by the nanometers of peak shift per refractive index unit and expressed in nm/RIU:

$$S(t) = \Delta\lambda(t) / \Delta n(t) \qquad (2)$$

Optics EXPRESS

Where Δλ(t) is the spectral shift of the resonance peak as a function of the thickness of the deposited SiO_2 layer. The second evaluates its precision and depends on the ratio of sensitivity S and the peak linewidth Δλ

$$FoM = S / \Delta\lambda \tag{3}$$

While the spectral shift and the linewidth of the plasmonic resonance can be experimentally measured, for the refractive index shift an analytical analysis has been done following the criteria reported in Ref [24]. It consists in treating the metal-SiO_2 material as Insulator-Metal multilayered metamaterial, whose overall effective dielectric function can be easily calculated applying the interface conditions for the electric field vector [36,37]. By using this approximation, it was possible to calculate the refractive index shift Δn(t) induced by the depositions of SiO_2.The results reported in Fig. 3(a) show an average sensitivity for the NPG array of 4000 nm/RIU, whereas the Au array reports at best 1000 nm/RIU. Moreover, in the case of the first layers of the SiO_2 (1.4 nm), the NPG reports a sensitivity that peaks at 7000 nm/RIU, 17 times higher than Au. The performances of NPG array against the Au counterpart are confirmed by the FoM in Fig. 3(b). The FoM of ranges between 20 (calculated for t_{SiO2} = 10.5nm) and 30 (calculated for t_{SiO2} = 1.4nm) for NPG and it is 6 times higher than Au. Here it is important to note that although the NPG array peak linewidth is depleted (due to the larger diameter of the antennas), the FoM remains unaffected.

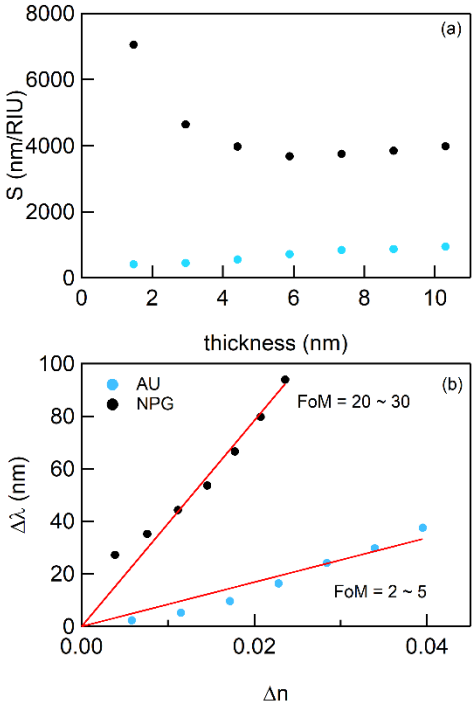

Fig. 3. (a) Sensitivity, expressed as nm/RIU, and (b) figures of merit of the NPG and homogenous Au arrays.

While the previous measurements can be used to evaluate the sensitivity of the platform, a real sensing application typically requires the detection of biomolecules at very low concentration. As in our previous experiments on NPG sensing [24], here we tested the performance of the material as a sensor by detecting low molecular weight proteins in solution. The detection approach was tested using different concentration of polyhistidine (7HIS), a small molecule (c.a. 1kDa).Obviously this approach can be successfully used also for the

Optics EXPRESS

detection of bigger molecules such as proteins [38]. The covalent linkage of the analyte to the surface allows a better and more trustable detection, which can be accomplished both in wet and dry configurations. The results of the resonance peak shifts performed by means of FTIR for concentrations of 7HIS between 10pM and 10nM are illustrated in Fig. 4. As in our previous experiments [24], by using this approach, a detection limit of 10 pM was verified. Noteworthy is the ability of the NPG antennas platform to detect the functional layer of APTES deposited by means of ALD as conformal uniform monolayer. As previously proved [24], the thickness of this organic monolayer (measured by means of XPS) results about 0.6 nm. We expect that successive incubations of NPG 3D antennas with increasing concentrations of 7-HIS lead to increasing saturation of functional sites. The polypeptide has an expected thickness about 1.4 nm, hence, in total we expect an analyte layer 2 nm thick with a coverage that depends on the 7HIS concentration and the linkage efficiency. In the frequency region of the antenna resonance the refractive indexes of 7HIS and APTES are 1.70 and 1.47, respectively. At a final concentration of 10nM, we observe a spectral shift comparable to that obtained for SiO_2 deposition (extrapolating the shift expected with 2 nm).

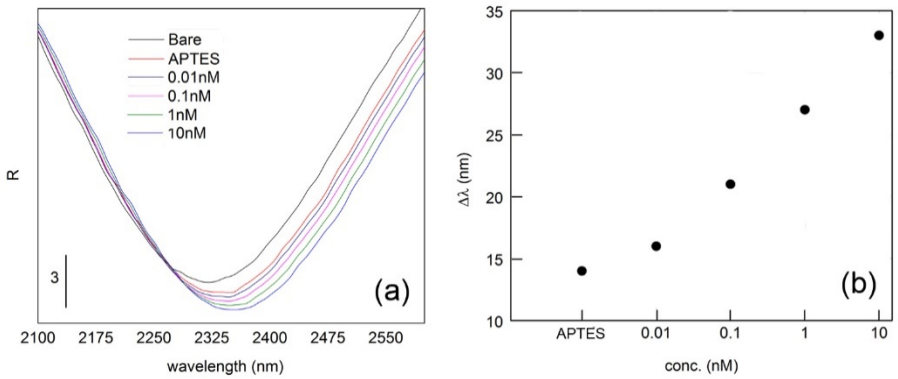

Fig. 4. Sensing performance of a bioanalyte. (a) Measured reflectance curves; (b) Spectral shifts.

The reported sensitivity can be explained by considering the plasmonic response of NPG in the NIR range. As illustrated in the authors' experiments [22–24], the field enhancement and confinement provided by the NPG at the metal/air or metal/liquid interface were much higher than what provided by the homogenous counterpart. This can be also a reasonable explanation for the observed higher sensitivity for the very first nm of functional layer (observed here and in our already mentioned work [24], both in the case of SiO_2 and APTES depositions). The porous structure, and the strong field confinement that rapidly decay above the very first nanometers of the NPG/air interface, enable a spontaneous co-localization of the plasmonic field and the analyte, thus promoting an effective interaction between them. This interaction results higher in the close proximity of the NPG surface, thus increasing the sensitivity to very small functional molecules/analytes. Of particular note, the sensitivity obtained with 3D antennas is significantly lower with respect to the one obtained on the NPG film monitoring the plasma edge shift. Compared to the NPG film sensitivity of 15,000 nm/RIU reported in [24], the one found for the here engineered nanostructure decreases down to 4,000 nm/RIU. Although this result need more investigations to be deeply understood, we suggest that it can be due to the absolute value of the dielectric function ε: approaching the plasma frequency (ω_p), the real part of ε approaches and cross the 0 line. At the same time the imaginary part of ε assume low values and the skin depth rapidly increases. Consequently: (i) the optical response (in terms of Δn) is more sensitive to the medium index changes and; (ii) the E field is able to probe the analyte molecule for all the film depth. Anyway, the main advantage of using plasmonic antennas is the possibility to finely tune the SPR over a broad spectral range modifying the geometric parameters of the array (pitch and antennas' height). The plasmonic

Optics EXPRESS

properties of NPG can be also tuned by different porosity [22–24], but with lower spectral accuracy.

4. Conclusion

In the present work we designed resonators exploiting plasmonic materials for IR sensing. Vertical NPG antennas with SPR in the NIR enable to detected small amount of analytes with sensitivity over 4000 nm/RIU. The enhanced sensitivity obtained with respect to the same nanostructures prepared with homogenous gold suggests that the effect is mainly due to the higher field confinement and enhancement observed with the porous substrate and not to its higher surface to volume ratio as previously proposed [39]. An easy and reproducibly fabrication strategy combined with the tunability of the optical properties of the material confirm that nanoporous gold patterns are promising tools for the realization of compact plasmonic platforms for sensing purposes.

References

1. J. N. Anker, W. P. Hall, O. Lyandres, N. C. Shah, J. Zhao, and R. P. Van Duyne, "Biosensing with plasmonic nanosensors," Nat. Mater. **7**(6), 442–453 (2008).
2. R. Semenyshyn, M. Hentschel, C. Stanglmair, T. Teutsch, C. Tarin, C. Pacholski, H. Giessen, and F. Neubrech, "In Vitro Monitoring Conformational Changes of Polypeptide Monolayers Using Infrared Plasmonic Nanoantennas," Nano Lett. **19**(1), 1–7 (2019).
3. D. Rodrigo, A. Tittl, N. Ait-Bouziad, A. John-Herpin, O. Limaj, C. Kelly, D. Yoo, N. J. Wittenberg, S.-H. Oh, H. A. Lashuel, and H. Altug, "Resolving molecule-specific information in dynamic lipid membrane processes with multi-resonant infrared metasurfaces," Nat. Commun. **9**(1), 2160 (2018).
4. M. E. Stewart, C. R. Anderton, L. B. Thompson, J. Maria, S. K. Gray, J. A. Rogers, and R. G. Nuzzo, "Nanostructured plasmonic sensors," Chem. Rev. **108**(2), 494–521 (2008).
5. G. Homola, S. S. Yee, and G. Gauglitz, "Surface plasmon resonance sensors: review," Sens. Actuators B Chem. **54**(1-2), 3–15 (1999).
6. M.-C. Estevez, M. A. Otte, B. Sepulveda, and L. M. Lechuga, "Trends and challenges of refractometric nanoplasmonic biosensors: a review," Anal. Chim. Acta **806**, 55–73 (2014).
7. G. Zanchetta, R. Lanfranco, F. Giavazzi, T. Bellini, and M. Buscaglia, "Emerging applications of label-free optical biosensors," Nanophotonics **6**(4), 627–645 (2017).
8. J. R. Mejía-Salazar and O. N. Oliveira, Jr., "Plasmonic Biosensing," Chem. Rev. **118**(20), 10617–10625 (2018).
9. H. Raether, Surface Plasmons on Smooth and Rough Surfaces and on Gratings, Springer Tracts in Modern Physics (Springer Berlin Heidelberg, 1988), 111.
10. J. Homola, I. Koudela, and S. S. Yee, "Surface plasmon resonance sensors based on diffraction gratings and prism couplers: sensitivity comparison," Sens. Actuators B Chem. **54**(1–2), 16–24 (1999).
11. A. E. Cetin, A. F. Coskun, B. C. Galarreta, M. Huang, D. Herman, A. Ozcan, and H. Altug, "Handheld high-throughput plasmonic biosensor using computational on-chip imaging," Light Sci. Appl. **3**, (2014).
12. C. Burda, X. Chen, R. Narayanan, and M. A. El-Sayed, "Chemistry and properties of nanocrystals of different shapes," Chem. Rev. **105**(4), 1025–1102 (2005).
13. E. M. Hicks, S. Zou, G. C. Schatz, K. G. Spears, R. P. Van Duyne, L. Gunnarsson, T. Rindzevicius, B. Kasemo, and M. Käll, "Controlling plasmon line shapes through diffractive coupling in linear arrays of cylindrical nanoparticles fabricated by electron beam lithography," Nano Lett. **5**(6), 1065–1070 (2005).
14. C. L. Haynes and R. P. Van Duyne, "Nanosphere Lithography: A Versatile Nanofabrication Tool for Studies of Size-Dependent Nanoparticle Optics," J. Phys. Chem. B **105**(24), 5599–5611 (2001).
15. E. Petryayeva and U. J. Krull, "Localized surface plasmon resonance: nanostructures, bioassays and biosensing--a review," Anal. Chim. Acta **706**(1), 8–24 (2011).
16. J. B. Lassiter, H. Sobhani, J. A. Fan, J. Kundu, F. Capasso, P. Nordlander, and N. J. Halas, "Fano resonances in plasmonic nanoclusters: geometrical and chemical tunability," Nano Lett. **10**(8), 3184–3189 (2010).
17. Y. Shen, J. Zhou, T. Liu, Y. Tao, R. Jiang, M. Liu, G. Xiao, J. Zhu, Z. K. Zhou, X. Wang, C. Jin, and J. Wang, "Plasmonic gold mushroom arrays with refractive index sensing figures of merit approaching the theoretical limit," Nat. Commun. **4**(1), 2381 (2013).
18. S. Zhang, K. Bao, N. J. Halas, H. Xu, and P. Nordlander, "Substrate-induced Fano resonances of a plasmonic nanocube: a route to increased-sensitivity localized surface plasmon resonance sensors revealed," Nano Lett. **11**(4), 1657–1663 (2011).
19. K. V. Sreekanth, Y. Alapan, M. ElKabbash, E. Ilker, M. Hinczewski, U. A. Gurkan, A. De Luca, and G. Strangi, "Extreme sensitivity biosensing platform based on hyperbolic metamaterials," Nat. Mater. **15**(6), 621–627 (2016).
20. A. V. Kabashin, P. Evans, S. Pastkovsky, W. Hendren, G. A. Wurtz, R. Atkinson, R. Pollard, V. A. Podolskiy, and A. V. Zayats, "Plasmonic nanorod metamaterials for biosensing," Nat. Mater. **8**(11), 867–871 (2009).
21. A. G. Brolo, "Plasmonics for future biosensors," Nat. Photonics **6**(11), 709–713 (2012).

Optics EXPRESS

22. D. Garoli, E. Calandrini, A. Bozzola, A. Toma, S. Cattarin, M. Ortolani, and F. De Angelis, "Fractal-Like Plasmonic Metamaterial with a Tailorable Plasma Frequency in the near-Infrared," ACS Photonics **5**(8), 3408–3414 (2018).
23. D. Garoli, E. Calandrini, A. Bozzola, M. Ortolani, S. Cattarin, S. Barison, A. Toma, and F. De Angelis, "Boosting infrared energy transfer in 3D nanoporous gold antennas," Nanoscale **9**(2), 915–922 (2017).
24. D. Garoli, E. Calandrini, G. Giovannini, A. Hubarevich, V. Caligiuri, and F. De Angelis, "Nanoporous gold metamaterials for high sensitivity plasmonic sensing," Nanoscale Horizons (2019). DOI: 10.1039/C9NH00168A.
25. P. R. Griffiths and J. A. De Haseth, Fourier transform infrared spectrometry Vol. 171. John Wiley & Sons, 2007.
26. B. Päivänranta, H. Merbold, R. Giannini, L. Büchi, S. Gorelick, C. David, J. F. Löffler, T. Feurer, and Y. Ekinci, "High aspect ratio plasmonic nanostructures for sensing applications," ACS Nano **5**(8), 6374–6382 (2011).
27. A. D. Mueller, L. Y. M. Tobing, and D. Hua Zhang, "Reliable Fabrication of High Aspect Ratio Plasmonic Nanostructures Based on Seedless Pulsed Electrodeposition," Adv. Mater. Technol. **4**(1), 1800364 (2019).
28. J. K. Gansel, M. Thiel, M. S. Rill, M. Decker, K. Bade, V. Saile, G. von Freymann, S. Linden, and M. Wegener, "Gold helix photonic metamaterial as broadband circular polarizer," Science **325**(5947), 1513–1515 (2009).
29. H. H. Huang and Y.-C. Hung, "Numerical analysis and the effective parameter retrieval of helical metamaterials," Phot. Phon. Prop. Eng. Nano. III **8632**, 863222 (2013).
30. M. Esposito, V. Tasco, F. Todisco, M. Cuscunà, A. Benedetti, M. Scuderi, G. Nicotra, and A. Passaseo, "Programmable Extreme Chirality in the Visible by Helix-Shaped Metamaterial Platform," Nano Lett. **16**(9), 5823–5828 (2016).
31. J. Kaschke and M. Wegener, "Optical and Infrared Helical Metamaterials," Nanophot. **5**(4), 510–523 (2016).
32. C. Marichy, M. Bechelany, and N. Pinna, "Atomic layer deposition of nanostructured materials for energy and environmental applications," Adv. Mater. **24**(8), 1017–1032 (2012).
33. M. M. Biener, J. Biener, A. Wichmann, A. Wittstock, T. F. Baumann, M. Bäumer, and A. V. Hamza, "ALD functionalized nanoporous gold: thermal stability, mechanical properties, and catalytic activity," Nano Lett. **11**(8), 3085–3090 (2011).
34. K. M. Mayer and J. H. Hafner, "Localized surface plasmon resonance sensors," Chem. Rev. **111**(6), 3828–3857 (2011).
35. K. A. Willets and R. P. Van Duyne, "Localized surface plasmon resonance spectroscopy and sensing," Annu. Rev. Phys. Chem. **58**(1), 267–297 (2007).
36. X. Chen, T. M. Grzegorczyk, B.-I. Wu, J. Pacheco, Jr., and J. A. Kong, "Robust method to retrieve the constitutive effective parameters of metamaterials," Phys. Rev. E Stat. Nonlin. Soft Matter Phys. **70**(1 Pt 2), 016608 (2004).
37. F.-G. Hu, J. Song, and T. Kamgaing, "Modeling of multilayered media using effective medium theory," in 19th Topical Meeting on Electrical Performance of Electronic Packaging and Systems (IEEE, 2010), pp. 225–228.
38. S. Barizuddin and S. G. S. Bok, "Plasmonic Sensors for Disease Detection - A Review," J. Nanomed. Nanotechnol. **7**(3), 1000373 (2016).
39. G. Ruffato, F. Romanato, D. Garoli, and S. Cattarin, "Nanoporous gold plasmonic structures for sensing applications," Opt. Express **19**(14), 13164–13170 (2011).